1521-009X/43/12/1872–1881$25.00
Drug Metabolism and Disposition
http://dx.doi.org/10.1124/dmd.115.066175
Drug Metab Dispos 43:1872–1881, December 2015

Atenolol Renal Secretion Is Mediated by Human Organic Cation Transporter 2 and Multidrug and Toxin Extrusion Proteins[S]

Jia Yin, Haichuan Duan, Yoshiyuki Shirasaka,[1] Bhagwat Prasad, and Joanne Wang

Department of Pharmaceutics, University of Washington, Seattle, Washington

Received July 3, 2015; accepted September 14, 2015

ABSTRACT

Atenolol is a β-blocker widely used in the treatment of hypertension. Atenolol is cleared predominantly by the kidney by both glomerular filtration and active secretion, but the molecular mechanisms involved in its renal secretion are unclear. Using a panel of human embryonic kidney cell lines stably expressing human organic cation transporter (hOCT) 1–3, human organic anion transporter (hOAT) 1, hOAT3, human multidrug and toxin extrusion protein (hMATE) 1, and hMATE2-K, we found that atenolol interacted with both organic cation and anion transporters. However, it is transported by hOCT1, hOCT2, hMATE1, and hMATE2-K, but not by hOCT3, hOAT1, and hOAT3. A detailed kinetic analysis coupled with absolute quantification of membrane transporter proteins by liquid chromatography–tandem mass spectrometry revealed that atenolol is an excellent substrate for the renal transporters hOCT2, hMATE1, and hMATE2-K. The K_m values for hOCT2, hMATE1, and hMATE2-K are 280 ± 4, 32 ± 5, and 76 ± 14 μM, respectively, and the calculated turnover numbers are 2.76, 0.41, and 2.20 s^{-1}, respectively. To demonstrate unidirectional transepithelial transport of atenolol, we developed and functionally validated a hOCT2/hMATE1 double-transfected Madin-Darby canine kidney cell culture model. Transwell studies showed that atenolol transport in the basal (B)-to-apical (A) direction is 27-fold higher than in the A-to-B direction, whereas its B-to-A/A-to-B transport ratio was only 2 in the vector-transfected control cells. The overall permeability of atenolol in the B-to-A direction in hOCT2/hMATE1 cells was 44-fold higher than in control cells. Together, our data support that atenolol tubular secretion is mediated through the hOCT2/hMATEs secretion pathway and suggest a significant role of organic cation transporters in the disposition of an important antihypertensive drug.

Introduction

Hypertension is a global health issue and a leading cause of cardiovascular disease, which contributes to 17 million deaths per year (World Health Organization, 2011). In addition to lifestyle changes, drug therapy is indispensable in the management of hypertension. There are several classes of antihypertensive drugs, and most patients need combination antihypertensive therapy to achieve blood pressure control (Whalen, 2015). Furthermore, patients with comorbidities may take multiple medications, which could lead to potentially adverse drug-drug interactions (DDIs).

Atenolol is the main β-blocker used alone or in combination to treat hypertension. It is also used to prevent angina and improve survival after a heart attack (Hernandez-Canero et al., 1972; Poirier and Lacourciere, 2012). Atenolol selectively blocks β1-adrenoceptors and reduces blood pressure mainly by decreasing cardiac output (Wadworth et al., 1991; Tabacova and Kimmel, 2002). Due to its hydrophilicity, atenolol does not pass through the blood-brain barrier, thus avoiding various central nervous system side effects (Agon et al., 1991). Less than 5% of the absorbed dose is bound to plasma protein. Atenolol is almost exclusively eliminated by the kidney, with more than 95% of the absorbed dose excreted unchanged in the urine (Brown et al., 1976; Mason et al., 1979). The total body clearance of atenolol correlates well with renal function, and a dosage adjustment is required in patients with impaired renal function (Agrawal et al., 2015). The reported renal clearance (~168 to ml/min) is larger than its glomerular filtration clearance (Mason et al., 1979; Goodman et al., 2011), suggesting that in addition to glomerular filtration, atenolol undergoes net tubular secretion.

In the human kidney, tubular secretion of drugs is mediated by the coordinated function of a number of drug transporters located in the basolateral and apical membranes of renal proximal tubular cells (Morrissey et al., 2013). Two major secretion systems exist for organic cation and organ anion drugs. In human kidneys, circulating organic cations are first transported into renal tubular cells by the electrogenic

This study was supported by the National Institutes of Health National Institute of General Medical Sciences [Grant R01 GM066233] and the National Center for Advancing Translational Sciences [Grant TL1 TR000422]. The content is solely the responsibility of the authors and does not necessarily represent the official views of the National Institutes of Health.

[1]Current affiliation: Department of Biopharmaceutics, Tokyo University of Pharmacy and Life Science, Hachioji, Tokyo, Japan.

dx.doi.org/10.1124/dmd.115.066175.

[S]This article has supplemental material available at dmd.aspetjournals.org.

ABBREVIATIONS: A, apical; ASP+, 4-[4-(dimethylamino)styryl]-*N*-methylpyridinium iodide; B, basal; DDI, drug-drug interaction; HEK, human embryonic kidney; hMATE, human multidrug and toxin extrusion protein; hOAT, human organic anion transporter; hOCT, human organic cation transporter; KRH, Krebs-Ringer-HEPES; LC-MS/MS, liquid chromatography–tandem mass spectrometry; MDCK, Madin-Darby canine kidney; OATP, organic anion transporting polypeptide; P-gp, P-glycoprotein; RFU, relative fluorescence unit; SIL, stable isotope labeled; TEER, transepithelial electrical resistance.

basolateral organic cation transporter (hOCT) 2, which is driven by the inside negative membrane potential. Once inside the cells, organic cations are further secreted into the urine by the apical multidrug and toxin extrusion proteins (hMATE) 1 and 2-K, which are proton/organic cation exchangers that use the inwardly directed proton gradient in the nephron to drive efflux (Motohashi and Inui, 2013). Organic anion drugs, on the other hand, are first transported into tubular cells by the basolateral organic anion transporters (hOATs) 1 and 3 (You, 2004; Burckhardt, 2012). Although hOAT1 and hOAT3 are generally selective for negatively charged molecules, hOAT3 is also able to transport certain positively charged drugs, such as cimetidine (Giacomini et al., 2010). Mechanisms of organic anion efflux at the apical membrane are less clear and may involve multiple transporters, including the multidrug resistance proteins 2 and 4.

Like many other β-blocker agents, atenolol has an oxypropanolamine group that is protonized at the secondary amine moiety. With a pKa of 9.6, atenolol primarily exists in the positively charged form at a physiologic pH (Martinez et al., 2000). Atenolol was previously shown to be a substrate of the hOAT polypeptide 1A2 (Kato et al., 2009). Intestinal organic anion transporting polypeptides (OATPs) are thought to play a role in atenolol oral absorption, and inhibition of intestinal OATPs by fruit juices has been proposed as the underlying mechanism of atenolol-fruit juice interactions in humans (Lilja et al., 2005; Jeon et al., 2013). In addition, there is also evidence that atenolol may be transported by the drug efflux transporter P-glycoprotein (P-gp) (Augustijns and Mols, 2004; Wang et al., 2005).

Little is currently known regarding the involvement of drug transporters in the renal handling of atenolol. Recently, Ciarimboli et al. showed that hOCTs interact with several β-blockers and may also accept some β-blockers as substrates (Ciarimboli et al., 2013). Based on the physiochemical property of atenolol and the known renal elimination mechanism of organ cations, we hypothesized that renal secretion of atenolol is mediated by the hOCT2/hMATEs pathway. The goal of this study is to elucidate the roles of hOCT2 and hMATE1/hMATE2-K in the renal transport of atenolol. To this end, we first characterized the interaction of atenolol with the major renal transporters hOCT2, hMATE1, hMATE2-K, hOAT1, and hOAT3 to identify transporters involved in renal handling of atenolol. Second, the detailed transport kinetics of atenolol was analyzed with identified transporters in conjunction with transporter protein quantification using a targeted liquid chromatography–tandem mass spectrometry (LC-MS/MS) proteomic approach. Finally, transporter-mediated unidirectional transport of atenolol was demonstrated in an in vitro model of organic cation renal secretion, hOCT2/hMATE1 double-transfected Madin-Darby canine kidney (MDCK) cells.

Materials and Methods

Materials. [^{3}H]atenolol (3.3 Ci/mmol) and [^{14}C]metformin (98 mCi/mmol) were purchased from Moravek Biochemicals, Inc. (Brea, CA). [^{3}H]estrone sulfate (50 Ci/mmol), [^{3}H]*para*-aminohippurate (3 Ci/mmol), and [^{3}H]mannitol (20 Ci/mmol) were purchased from American Radiolabeled Chemicals, Inc. (St. Louis, MO). Nonradiolabeled compounds were purchased from Sigma-Aldrich (St. Louis, MO) and were of analytical grade. Synthetic signature peptides (Supplemental Table 1) for protein quantification were obtained from New England Peptides (Boston, MA). The corresponding stable isotope labeled (SIL) internal standards were obtained from Thermo Fisher Scientific (Rockford, IL). Cell culture media and reagents were purchased from Invitrogen (Carlsbad, CA).

Cell Culture. Flp-In human embryonic kidney (HEK) 293 cells stably transfected with transporters and the pcDNA5/FRT vector were maintained in Dulbecco's modified Eagle's medium (high glucose) supplemented with 10% fetal bovine serum, 2 mM L-glutamine, 100 U/ml penicillin, 100 μg/ml streptomycin, and 150 μg/ml hygromycin B. For better attachment of Flp-In 293 cells, cell culture plastic surfaces were coated with 0.01% poly-D-lysine in phosphate-buffered saline. MDCK cells transfected with empty vectors or double-transfected with hOCT2 and hMATE1 were maintained in minimum essential medium supplemented with 10% fetal bovine serum, 500 μg/ml G418, and 200 μg/ml hygromycin B. Cells were cultured in a 37°C humidified incubator with 5% CO_2.

Generation of HEK293 Cell Lines Stably Expressing Transporters. To generate HEK293 cell lines stably expressing various transporters at isogenic locations, the Flp-In system from Invitrogen was used as we previous described for hOCT3 (Duan and Wang, 2010). The same procedure was used to generate HEK293 cell lines stably expressing hOCT1, hOCT2, hMATE1, hMATE2-K, hOAT1, and hOAT3. The cDNAs encoding hOCT1 (*SLC22A1*) and hOCT2 (*SLC22A2*) were amplified from human liver and kidney mRNA by real-time polymerase chain reaction as previously described (Duan and Wang, 2010). The cDNAs encoding hOAT1 (*SLC26A6*) and hOAT3 (*SLC26A8*) were previously developed in our laboratory (Li et al., 2006). The hMATE1 (*SLC47A1*) plasmid was purchased from GE Dharmacon (Lafayette, CO), and the hMATE2-K plasmid was kindly provided to us by Dr. Kazuo Matsubara of Kyoto University (Kyoto, Japan) (Masuda et al., 2006). The insert encoding a transporter was then subcloned into the pcDNA5/FRT vector by polymerase chain reaction amplification, restriction enzyme digestion, and ligation. The cDNA sequences of all inserts were verified by DNA sequencing and compared with National Center for Biotechnology Information reference genes (BC126364.1 for hOCT1, BC039899.1 for hOCT2, NM_153276.2 for hOAT1, NM_004254.3 for hOAT3, NM_018242.2 for hMATE1, and NM_001099646.1 for hMATE2-K) to ensure fidelity. The constructs were then cotransfected with the pOG44 Flp-recombinase expression vector (Invitrogen) into the Flp-In HEK293 cells. Transfected cells were selected by hygromycin B (150 μg/ml) and expanded. The pcDNA5/FRT empty vector was also cotransfected with pOG44 into the Flp-In HEK293 cells to serve as control cells.

Generation of hOCT2/hMATE1 Double-Transfected MDCK Cells. hOCT2/hMATE1 MDCK cells were generated through double-transfection followed by antibiotic selection and activity screening. The hOCT2 and hMATE1 pcDNA5/FRT constructs were developed as described above. The full-length cDNA encoding hOCT2 was then subcloned into the pcDNA3.1+ mammalian expression vector (Life Technologies, Carlsbad, CA). The cDNA encoding hMATE1 was then subcloned into the pcDNA3.1/Hygro(+) expression vector. The new constructs were cotransfected at a 1:1 molar ratio into MDCK cells. Transfected cells were selected by G418 (500 μg/ml) and hygromycin B (200 μg/ml) for 3 to 4 weeks. Colonies with normal cellular morphology and growth rate were isolated and expanded. The cell colonies were screened in functional transport assays by determining B-to-A and A-to-B permeability of [^{14}C]metformin as described below. Tight junction formation in transfected MDCK monolayers was assessed by measuring the permeability of [^{3}H]mannitol. A colony with the highest metformin B-to-A/A-to-B ratio but low and similar B-to-A and A-to-B mannitol permeability was selected and used in transport studies. A control cell line cotransfected with empty pcDNA3.1+ and pcDNA3.1/Hygro(+) vectors at a 1:1 molar ratio was obtained using similar transfection and selection procedures.

Uptake and Inhibition Assays in HEK293 Cells. The assays were performed as previously described (Duan and Wang, 2010), with some modifications. Control cells and transporter-expressing cells were seeded in poly-D-lycine–coated 24-well plates and allowed to grow for 2 to 3 days to reach 80–90% confluence. Uptake assays were performed at 37°C in Krebs-Ringer-HEPES (KRH) buffer (5.6 mM glucose, 125 mM NaCl, 4.8 mM KCl, 1.2 mM KH_2PO_4, 1.2 mM $CaCl_2$, 1.2 mM $MgSO_4$, and 25 mM HEPES) containing cold substrates and trace amounts of radiolabeled substrates. For uptake studies in hMATE1- and hMATE2-K–expressing cells, KRH buffer was adjusted to pH 8.0 to generate an outwardly directed proton gradient since these transporters function as proton/organic cation exchangers (Otsuka et al., 2005). For all other transporters, uptake was performed at pH 7.4. After incubating the cells with a substrate for a specified time, uptake was terminated by washing cells three times with ice-cold KRH buffer. Cells were then solubilized with 0.5 ml 1 M NaOH at 37°C for 2 hours and neutralized with 0.5 ml 1 M HCl. Radioactivity of cell lysates was measured by a liquid scintillation counter (Tri-Carb B3110TR; PerkinElmer, Waltham, MA). For atenolol inhibition studies, uptake was performed in the presence of atenolol (500 μM). Protein content in the lysates was measured by the BCA protein

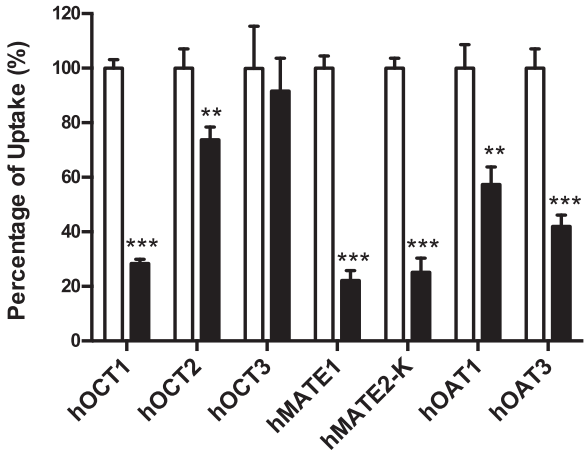

Fig. 1. Inhibitory effect of atenolol on the uptake of probe substrates by selected drug transporters. Uptake of 6.1 μM metformin by hOCT1, hOCT2, hOCT3, hMATE1, and hMATE2-K, 2 μM *para*-aminohippurate by hOAT1, and 0.06 μM estrone sulfate by hOAT3 in the absence and presence of 500 μM atenolol was measured in both transporter-expressing and control HEK293 cells. Transporter-specific uptake was obtained by subtracting the uptake in control cells from the uptake in transporter-expressing cells. The uptake in the absence of atenolol (unfilled) was set as 100%. The uptake in the presence of atenolol (filled) was expressed as a percentage of the uptake in the absence of atenolol. The uptake was measured after a 2-minute incubation at 37°C. Data are presented as the mean ± S.D. Uptake in the presence of atenolol was compared with that in the absence of atenolol (**$P < 0.01$; ***$P < 0.001$).

assay kit (Pierce Chemical, Rockford, IL) and the uptake in cells was normalized to their protein concentrations. Transporter-specific uptake was calculated by subtracting the background uptake in the control cells.

Atenolol Inhibition Study Using a Fluorescent Substrate. 4-[4-(Dimethylamino)styryl]-*N*-methylpyridinium iodide (ASP+) is a fluorescent analog of MPP+ (1-methyl-4-phenylpyridinium) that has been used as a probe substrate to determine ligand-transporter interaction using fluorescence-based assays (Mason et al., 2005). Uptake was performed with an ASP+ cocktail (2 μM ASP+ and 10 μM Trypan blue in KRH buffer) using a previously described procedure (Ahlin et al., 2008; Duan et al., 2015). pcDNA5 control cells and transporter-expressing cells were seeded in poly-D-lycine–coated 96-well plates and grown for 48 hours until approximately 90% confluence. The experiment was initiated by incubating cells with the ASP+ cocktail at 37°C, and the relative fluorescence unit (RFU) was measured immediately (time 0) and at various time points (5, 10, and 15 minutes) using a PerkinElmer Wallac 1420 Multilabel counter, with excitation/emission wavelengths of 475/609 nm. Specific uptake was calculated by subtracting the RFU at time 0 from the RFU at the end point ($RFU_{end} - RFU_0$). ASP+ uptake was measured at various times to determine the initial uptake range, and a time point within the linear range was chosen as the time point for inhibition studies. For inhibition studies with atenolol stereoisomers, the cells were preincubated with each isomer and uptake was performed in the presence of the stereoisomers at varying concentrations.

Transport Studies in hOCT2/hMATE1 Double-Transfected MDCK Cells. Atenolol flux across the MDCK monolayer expressing hOCT2/hMATE1 was determined using a previously described protocol, with some modifications (Muller et al., 2013). MDCK cells were seeded on Falcon cell culture inserts at a density of $2 \times 10^5/cm^2$. Five days after seeding, transport experiments were performed. After removing the culture medium from both sides of the inserts, cells were preincubated for 10 minutes at 37°C in KRH buffer, with the pH adjusted to pH 6.0 and 7.4, respectively, at the apical and basal chamber. For A-to-B transport, 2 ml of KRH buffer (pH 7.4) was added to the basal chamber, and transport was initiated by adding 0.8 ml of the KRH buffer (pH 6.0) containing [^{3}H]atenolol (1 μM) to the apical chamber. For B-to-A transport, 0.8 ml of KRH buffer (pH 6.0) was added to the apical chamber and 2 ml of KRH buffer (pH 7.4) containing [^{3}H]atenolol (1 μM) was added to the basal chamber. The use of an apical pH of 6.0 was based on the average urine pH of 6.3 as well as previously published methods by other groups (Tsuda et al., 2009; Roland and Tozer, 2010; Muller et al., 2011). To measure transcellular transport, an aliquot of the incubation medium (100 μl from the basal chamber and 50 μl from the apical chamber) in the receiving chamber was periodically collected and replaced with an equal volume of fresh buffer. At the end of the transport study, intracellular drug accumulation was measured by rinsing inserts three times with ice-cold KRH buffer (pH 7.4) followed by cell lysis with 1 M NaOH and then neutralization with 1 M HCl. The radioactivity of the collected medium and cell lysate was determined by a liquid scintillation counter (Tri-Carb B3110TR; PerkinElmer). Protein concentrations in the cell lysate were measured by a BCA protein assay kit (Pierce Chemical). The tightness of the MDCK monolayer was verified by measuring [^{3}H]mannitol permeability and transepithelial electrical resistance (TEER) using a Millicell-ERS system (Millipore Corporation, Bedford, MA) before and after each experiment to ensure monolayer integrity. Data generated in the MDCK cells with a TEER value $< 180\ \Omega \cdot cm^2$ were not accepted.

Membrane Protein Preparation and LC-MS/MS Quantification of Transporter Protein. Total membrane proteins were prepared from transporter-transfected HEK293 cells and MDCK cells using the ProteoExtract native membrane protein extraction kit (Calbiochem/EMD Millipore, San Diego, CA). The total membrane protein concentration was determined by the BCA protein assay kit (Pierce Chemical). To quantify the membrane transporter protein in each cell line, an LC-MS/MS proteomic approach (Lee et al., 2013; Prasad and Unadkat, 2014) was used. The Agilent 6460A triple quadrupole mass spectrometer coupled to the Agilent 1290 Infinity LC system (Agilent Technologies, Santa Clara, CA) operated in the ESI Electrospray ionization positive ionization mode and was used for LC-MS/MS analysis of the peptides (Supplemental Table 1). Approximately 1.5 μg or less of the trypsin digest (5 μl) was injected onto the column (Kinetex 2.6 μm, C18, 100 × 3 mm; Phenomenex, Torrance, CA) and eluted at 0.3 ml/min. The mobile phase gradient conditions were 97% A (0.1% v/v formic acid) and 3% B (acetonitrile containing 0.1% v/v formic acid) and held for 2.5 minutes, followed by three steps of linear gradient of mobile phase B concentrations of 3–8%, 8–21%, and 21–30%. Thirty percent mobile phase B was maintained for 2 minutes. This was followed by a washing step using 80% mobile phase B for 1.6 minutes and re-equilibration for 3.3 minutes. The doubly/triply charged parent to singly charged product transitions for the analyte peptides and their respective SIL peptides were monitored using optimized LC-MS/MS parameters (Supplemental Table 1). The data were processed by integrating the peak areas generated from the reconstructed ion chromatograms for the analyte peptides and the respective SIL internal standards using MassHunter software V (Agilent Technologies).

Data Analysis. All uptake experiments were performed in triplicate and repeated at least two times. Data were presented as mean ± S.D. ($n \geq 3$). The transport kinetics data were fitted through nonlinear regression using GraphPad Prism 6.0 (GraphPad Software, Inc., La Jolla, CA). The K_m and V_{max} values were obtained by fitting the data to the Michaelis-Menten equation $V = V_{max} * S/(K_m + S)$, where V is the velocity of uptake, V_{max} is the maximum velocity of uptake, S is

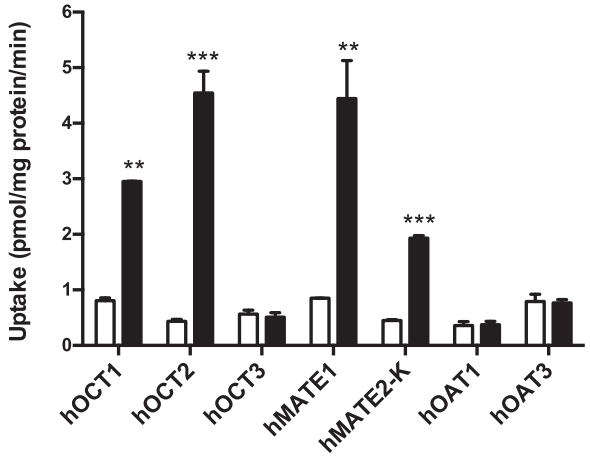

Fig. 2. Uptake of atenolol by selected drug transporters. The uptake of 1 μM atenolol in transporter-expressing (filled) and control (unfilled) HEK293 cells was measured. The uptake was measured after a 2-minute incubation at 37°C. Data are presented as the mean ± S.D. Uptake in transporter-expressing cells was compared with that in control cells (**$P < 0.01$; ***$P < 0.001$).

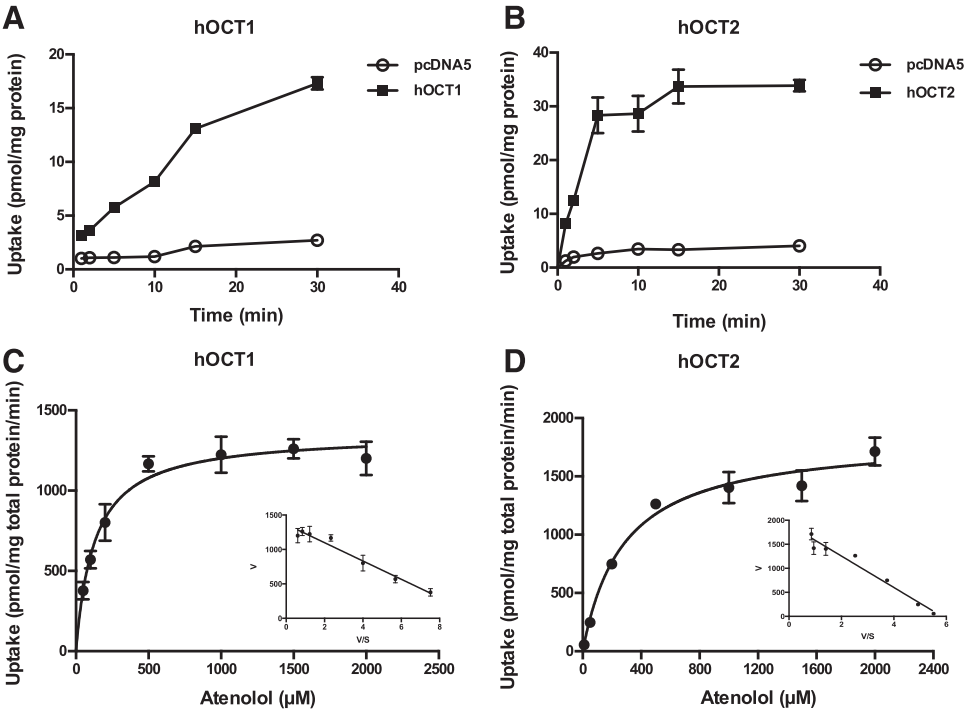

Fig. 3. Atenolol uptake kinetics by hOCT1 and hOCT2. The uptake of 1 μM atenolol was measured in control and transporter-expressing HEK293 cells at specified time points (A and B). Concentration-dependent uptake of atenolol was measured in both transporter-expressing and control HEK293 cells after a 2-minute incubation at 37°C (C and D). Transporter-specific uptake was obtained by subtracting the uptake in control cells from the uptake in transporter-expressing cells. Data were fitted with the Michaelis-Menten equation using nonlinear regression. The insets are the Eadie-Hofstee transformation of the kinetics data. Each data point represents the mean ± S.D.

the substrate concentration, and K_m is the Michaelis-Menten constant. In addition, kinetic data fitting was also performed using a Michaelis-Menten equation plus a diffusional component. The transporter turnover number (k_{cat}) was obtained by normalizing V_{max} to the amount of transporter protein quantified. The IC_{50} values were obtained by fitting data with log (inhibitor concentration) versus the normalized response using the equation $V = \text{Bottom} + (\text{Top} - \text{Bottom}) / [1 + (I/IC_{50})^{nH}]$, where V is the rate of uptake in the presence of inhibitor, bottom is the residual noninhibitable baseline value, top is the rate of uptake in the absence of the inhibitor, I is the inhibitor concentration, and nH is the Hill coefficient. For transport experiments, under the assumption that the substrate concentration at the donor side is constant, the apparent permeability (P_{app}) of compounds across cell monolayers was calculated as $P_{app} = (dQ/dt)/(A*C_0)$, where Q is the amount of compound transported over time t, A is the insert membrane surface area, and C_0 is the initial compound concentration in the donor chamber. Statistic analysis was performed using an unpaired Student's t test, and a P value of less than 0.05 was considered statistically significant.

Results

Functional Validation of Transporter-Expressing Cell Lines. The HEK293 cell line, which has negligible expression of endogenous organic cation and anion transporters (Ahlin et al., 2009), was used to generate various stable cell lines expressing major organic solute transporters using the Flp-In system. To assess the activity of the expressed transporters, uptake of a probe substrate was measured in both pcDNA5 (control) and transporter-expressing cell lines. Metformin was used for hOCT1–hOCT3 and hMATE1/hMATE2-K; *para*-aminohippurate was used for hOAT1; and estrone sulfate was used for hOAT3. Compared with the control cells (Supplemental Fig. 1), significantly enhanced uptake activity was observed for all transporter-expressing cells, demonstrating that all transporters are functionally expressed in the HEK293 cell lines used in this study.

Inhibitory Effect of Atenolol on Selected Drug Transporters. To determine if atenolol interacts with hOCT1, hOCT2, hOCT3, hMATE1, hMATE2-K, hOAT1, and hOAT3, the uptake of a probe substrate in the presence and absence of atenolol (500 μM) was measured in both control and transporter-expressing cells. The uptake in the presence of atenolol was expressed as a percentage of the specific uptake in the absence of atenolol. As shown in Fig. 1, atenolol at 500 μM inhibited hOCT1, hMATE1, and hMATE2-K by about 70%. Less but significant inhibition was also observed for hOCT2, hOAT1, and hOAT3. hOCT3 showed no interaction with atenolol.

Uptake of Atenolol by Selected Drug Transporters. To determine if atenolol is a substrate of the seven selected transporters, uptake of ^{3}H-labeled atenolol (1 μM) was measured in both control cells and transporter-expressing cells. Compared with vector-transfected cells, atenolol uptake was significantly increased in cells expressing hOCT1, hOCT2, hMATE1, and hMATE2-K (Fig. 2). Cells expressing hOCT2 and hMATE1 showed the highest uptake activity toward atenolol. In contrast, no significant uptake of atenolol was observed in cells expressing hOCT3, hOAT1, or hOAT3.

Atenolol Uptake Kinetics by hOCT1 and hOCT2. To determine the kinetics of atenolol uptake by hOCT1 and hOCT2, time-dependent uptake of atenolol (1 μM) was performed in KRH buffer (pH 7.4) at 37°C. Uptake in hOCT1- and hOCT2-expressing cells was linear for up to 15 and 5 minutes, respectively (Fig. 3, A and B). Concentration-dependent uptake was then performed at a 2-minute incubation time, and specific uptake was obtained by subtracting uptake in the control cells. hOCT1- and hOCT2-specific atenolol uptake was saturable, and the K_m values derived from nonlinear regression fitting to the Michaelis-Menten equation were 128 ± 16 and 280 ± 41 μM,

TABLE 1

Kinetic parameters of atenolol uptake by hOCT1, hOCT2, hMATE1, and hMATE2-K

	K_m	V_{max}
	μM	pmol/min/mg protein
hOCT1	128 ± 16	1355 ± 40
hOCT2	280 ± 41	1836 ± 71
hMATE1	32 ± 5	323 ± 12
hMATE2-K	76 ± 14	500 ± 22

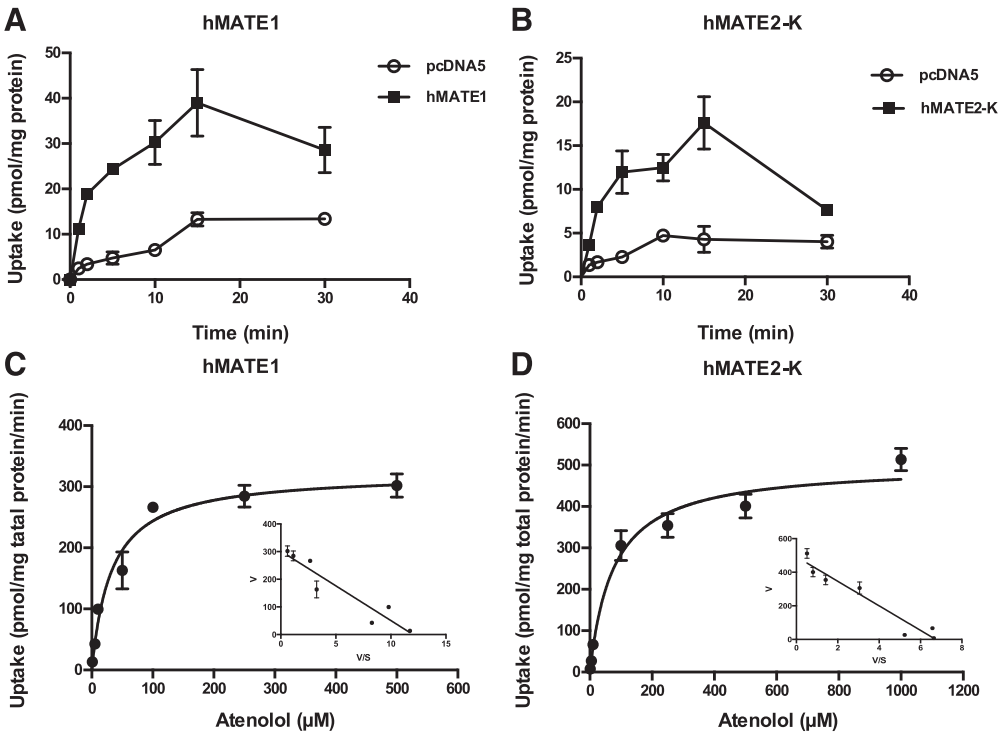

Fig. 4. Atenolol uptake kinetics by hMATE1 and hMATE2-K. The uptake of 1 μM atenolol was measured in control and transporter-expressing HEK293 cells at specified time points (A and B). Concentration-dependent uptake of atenolol was measured in both transporter-expressing and control HEK293 cells after a 2-minute incubation at 37°C (C and D). Transporter-specific uptake was obtained by subtracting the uptake in the control cells from the uptake in the transporter-expressing cells. Data were fitted with the Michaelis-Menten equation using nonlinear regression. The insets are the Eadie-Hofstee transformation of the kinetics data. Each data point represents the mean ± S.D.

respectively (Fig. 3, C and D; Table 1). The Eadie-Hofstee plots were consistent with single-enzyme kinetics (Fig. 3, C and D insets). In addition, we also fitted the kinetic data by adding a first-order diffusional component to the Michaelis-Menten equation. The resulting K_m and V_{max} values were essentially the same since diffusion was negligible due to subtraction of uptake in vector-transfected cells (Supplemental Table 2).

Atenolol Transport Kinetics by hMATE1 and hMATE2-K. Atenolol transport kinetics toward the renal efflux transporters hMATE1 and hMATE2-K were determined using uptake assays in KRH buffer at pH 8.0 to provide an outwardly directed proton gradient. This method has been used previously to measure the transport kinetics for the MATE transporters (Otsuka et al., 2005; Muller et al., 2013). Uptake increased progressively until 15 minutes, but declined at 30 minutes in both hMATE1- and hMATE2-K–transfected cells (Fig. 4, A and B), probably due to the dissipation of the proton gradient with time. Because uptake was linear within 2 minutes, concentration-dependent uptake was performed at 2 minutes. hMATE1- and hMATE2-K–mediated atenolol uptake was saturable (Fig. 4, C and D) with the K_m and V_{max} values shown in Table 1 and Supplemental Table 2. Compared with hOCT2, hMATE1 and hMATE2-K showed 4- to 9-fold higher affinity toward atenolol.

Transporter Quantification and Turnover Number Determination. To determine atenolol transport efficiency at the single transporter level, we quantified transporter protein expression levels in membrane fractions prepared from transfected HEK293 cell lines using targeted LC-MS/MS proteomics. The hOCT1, hOCT2, hMATE1, and hMATE2-K expression in HEK293 cell lines varied within 4-fold, and the protein levels for each transporter are shown in Table 2. The transporter turnover number (k_{cat}), which is the maximum number of substrates that can be transported during a transport cycle, was calculated by normalizing V_{max} to the number of transporters determined (Table 2). When single transporter efficiency (k_{cat}/K_m) was compared, hOCT2 and hMATE1 showed a similar transport efficiency for atenolol. hOCT1 and hMATE2-K had similar transport efficiencies, which were about three times higher than those of hOCT2 and hMATE1.

Inhibition of hOCT2, hMATE1, and hMATE2-K by *R*- and *S*-Atenolol. Like many other beta-blockers, atenolol has two stereoisomers. To evaluate if *R*- and *S*-atenolol have different affinities toward hOCT1, hOCT2, hMATE1, and hMATE2-K, the inhibitory effects of *R*- and *S*-atenolol on these transporters were determined using a rapid fluorescent substrate uptake assay. As shown in Fig. 5 and Table 3, the IC_{50} values of *R*- and *S*-atenolol for all four transporters were very similar, with a less than 25% difference, suggesting that hOCT1, hOCT2, hMATE1, and hMATE2-K have little steroselectivity for *R*- and *S*-atenolol.

Establishment of a hOCT2/hMATE1 Double-Transfected MDCK Cell Line. Double-transfected MDCK cells stably expressing hOCT2/hMATE1 were previously shown as a useful model to elucidate the vectorial transport pathway for organic cations (Sato et al., 2008; Konig et al., 2011). To demonstrate unidirectional transcellular transport of atenolol, we generated a MDCK cell line stably expressing

TABLE 2

Turnover number and transport efficiency of atenolol uptake by hOCT1, hOCT2, hMATE1, and hMATE2-K

	Amount of Transporter	k_{cat}	k_{cat}/K_m
	fmol/μg membrane	s^{-1}	$s^{-1}*\mu M^{-1}$
hOCT1	19.0 ± 0.02	4.57	36×10^{-3}
hOCT2	41.1 ± 3.6	2.76	9.9×10^{-3}
hMATE1	36.9 ± 4.8	0.41	12.8×10^{-3}
hMATE2-K	9.7 ± 1.3	2.20	28.9×10^{-3}

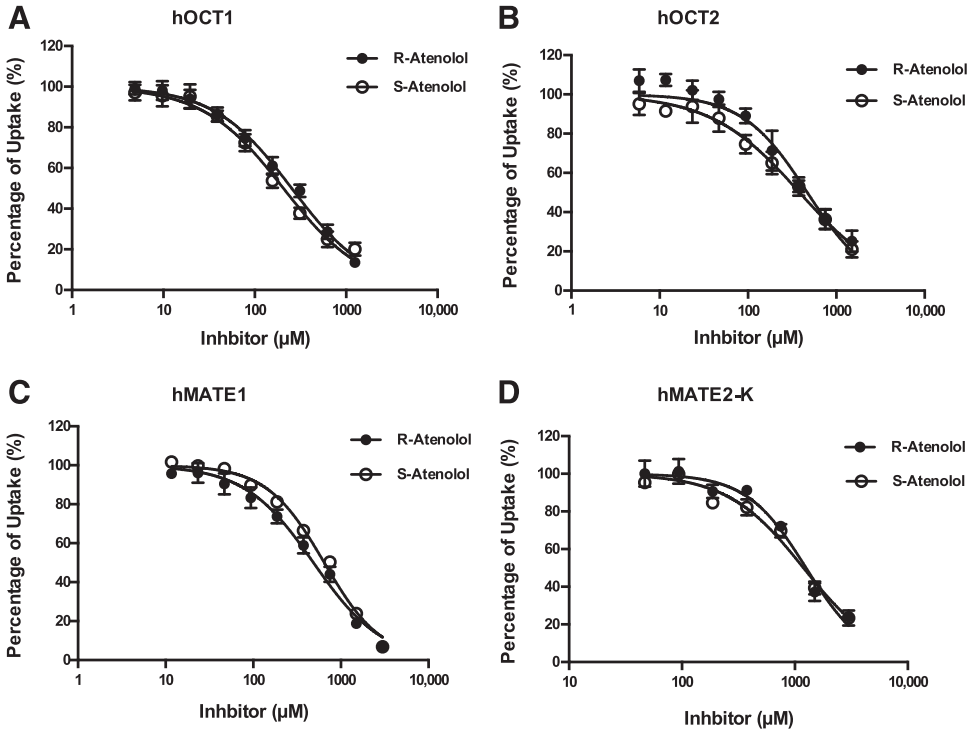

Fig. 5. Inhibition of hOCT1, hOCT2, hMATE1, and hMATE2-K by *R*- and *S*-atenolol. Uptake of 1 μM ASP+ in the absence and presence of *R*- and *S*-atenolol was measured in both transporter-expressing and control HEK cells. The uptake of ASP+ in the presence of *R*- and *S*-atenolol was expressed as a percentage of the uptake in the absence of *R*- and *S*-atenolol. Five minutes was chosen as the end point for specific uptake. Each data point represents the mean ± S.D.

hOCT2 and hMATE1. The membrane expression of hOCT2 and hMATE1 in these cells was quantified using LC-MS/MS. The hOCT2 and hMATE1 protein levels determined were 28.6 and 6.9 fmol/μg membrane protein, respectively. We then evaluated the barrier properties of the double-transfected cells by measuring TEER and transcellular transport of mannitol, a model compound for paracellular diffusion. The flux of mannitol was very low and similar in both the B-to-A and A-to-B directions in double-transfected and control cells (Fig. 6, A and B). There was no statistical difference in mannitol transport between the B-to-A and A-to-B directions at all time points except the last sampling point (120 minutes). However, the difference at 120 minutes is very small and showed an opposite direction in the vector and hOCT2/hMATE1-transfected cells. The calculated mannitol permeability was about 1.6×10^{-6} cm/s, which is in the reported range of 0.4×10^{-6} cm/s to 3.5×10^{-6} cm/s in polarized MDCK monolayer culture (Avdeef, 2010). The TEER values measured ranged from 180 to 200 $\Omega \cdot cm^2$, which are also within the reported range (Dukes et al., 2011). These data suggest the proper formation of tight junctions and the integrity of the barrier function in our transfected cell lines. The B-to-A transport of metformin, a widely used probe substrate for organic cation transporters, was much greater (up to 65-fold at 120 minutes) than A-to-B transport in the hOCT2/hMATE1 double-transfected cells (Fig. 6C). The B-to-A/A-to-B ratio at 30 minutes is estimated to be 56, which is similar to what was reported by Sato et al. (2008). In contrast, control cells showed much lower metformin transport in both directions and there was little difference between A-to-B and B-to-A flux (Fig. 6D).

Transcellular Transport of Atenolol in hOCT2/hMATE1-Transfected MDCK Cells. To determine the role of hOCT2 and hMATE1 in unidirectional transport of atenolol, time-dependent flux of [^{3}H]atenolol was examined using hOCT2/hMATE1-transfected MDCK cells. Transport studies were performed under pH gradient conditions (apical pH 6.0 and basal pH 7.4) based on physiologic conditions. As shown in Fig. 7A, transport of atenolol in the B-to-A direction was much greater than in the A-to-B direction in double-transfected cells. In contrast, transport of atenolol in the vector-transfected control cell was much slower in both directions and was only slightly higher in the B-to-A direction (Fig. 7B). Although MDCK cells have a generally negligible expression of many endogenous drug transporters, low expression of canine P-gp and OCT2 was reported (Shu et al., 2001; Kuteykin-Teplyakov et al., 2010). The slightly higher transport of atenolol in the B-to-A direction in the control cells is probably due to the expression of these endogenous transporters, which may also accept atenolol as a substrate. In both control and hOCT2/hMATE1 cells, the atenolol flux rate was constant over 120 minutes. Based on the time course, atenolol permeability was subsequently calculated and is shown in Fig. 7C. In hOCT2/hMATE1-transfected cells, the atenolol B-to-A/A-to-B permeability ratio was 27, whereas that in control cells was only 2. The overall permeability of atenolol in the B-to-A direction was 44-fold higher in hOCT2/hMATE1-transfected cells than in control cells. Intracellular accumulation of atenolol was measured at the end of the transport study. The hOCT2/hMATE1-transfected cells showed higher intracellular accumulation than control cells in both directions, and the B-to-A accumulation was higher than A-to-B in both cell lines (Fig. 7D).

Discussion

Despite the critical role of the kidney in atenolol disposition, the molecular mechanisms involved in the renal handling of atenolol have not been well understood. In this study, we characterized the interaction

TABLE 3

IC_{50} of *R*- and *S*-atenolol inhibition of ASP+ uptake by hOCT1, hOCT2, hMATE1, and hMATE2-K

Transporter	*R*-Atenolol IC_{50}	*S*-Atenolol IC_{50}	Ratio[a]	*P* value
	μM	μM		
hOCT1	254.1 ± 11.9	206.1 ± 11.4	1.2	< 0.05
hOCT2	470.0 ± 15.2	384.0 ± 20.6	1.2	< 0.05
hMATE1	486.9 ± 22.1	645.2 ± 41.4	0.8	< 0.05
hMATE2-K	1258 ± 101.9	1194 ± 117.6	1.1	0.52

[a]Ratio = *R*-atenolol IC_{50}/*S*-atenolol IC_{50}.

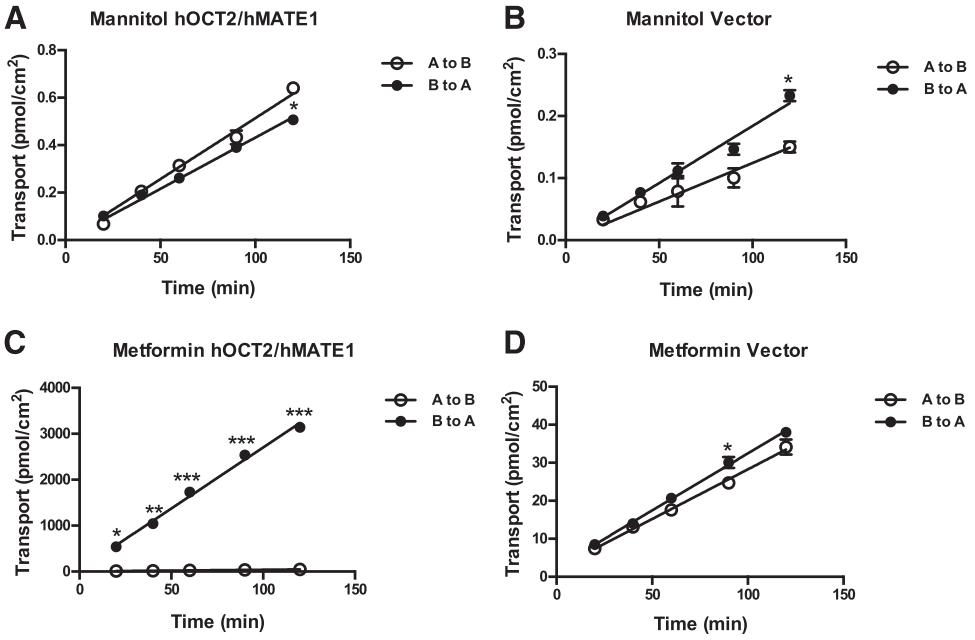

Fig. 6. Transcellular flux of mannitol and metformin in hOCT2/hMATE1 double-transfected and control MDCK cells. Cells were incubated in KRH buffer containing 0.05 μM mannitol (A and B) and 5.5 μM metformin (C and D) in either the apical (open circle) or basal (closed circle) chamber. An aliquot of buffer was taken periodically from the receiving chamber (100 μl from the basal chamber and 50 μl from the apical chamber) and radioactivity was subsequently measured. The pH of the apical and basal chambers was 6.0 and 7.4, respectively. Data were fitted with linear regression. Each data point represents the mean ± S.D. Transport in the basal-to-apical direction was compared with that in the apical-to-basal direction ($^{*}P < 0.05$; $^{**}P < 0.01$; $^{***}P < 0.001$). A to B, apical to basal; B to A, basal to apical.

of atenolol with major renal drug transporters and showed that atenolol is an excellent substrate for hOCT2, hMATE1, and hMATE2-K in single transfected HEK cells. Atenolol is an inhibitor, but not a substrate, for hOAT1 and hOAT3. Using a double-transfected MDCK monolayer culture, we further demonstrated the unidirectional transepithelial flux of atenolol mediated by hOCT2/hMATE1. Together, our data support that tubular secretion of atenolol in the kidney is mediated by the hOCT2/hMATEs secretion pathway, as depicted in Fig. 8.

While atenolol interacted with both organic cation and anion transporters, it was only transported by hOCT1, hOCT2, hMATE1, and hMATE2-K (Figs. 1 and 2), which is consistent with the drug

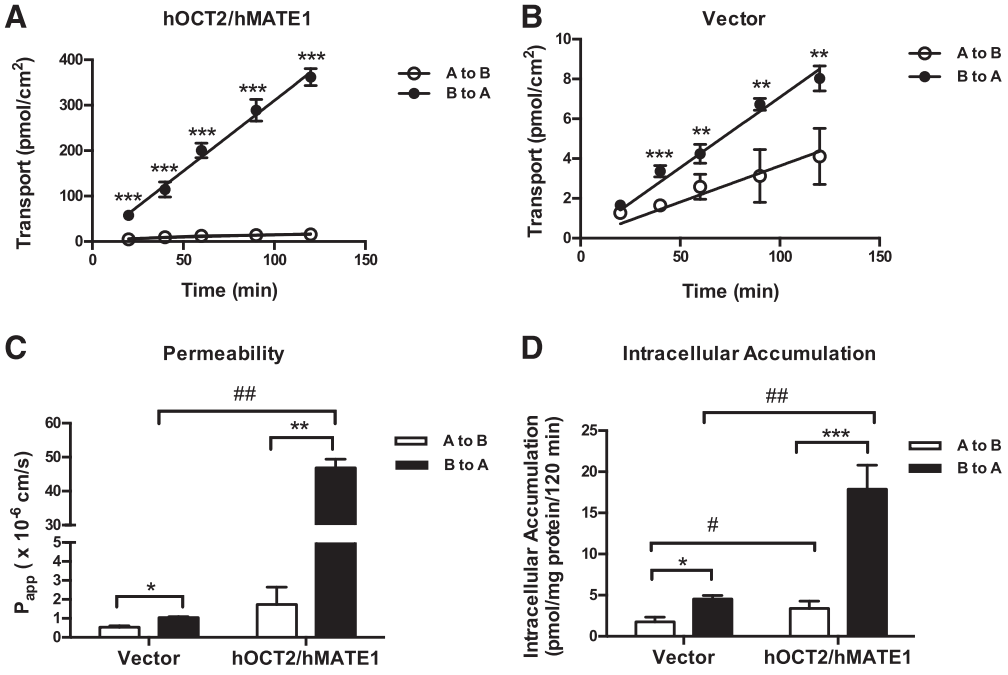

Fig. 7. Transcellular flux, permeability and intracellular accumulation of atenolol in hOCT2/hMATE1 double-transfected and control MDCK cells. Cells were incubated in KRH buffer containing 1 μM atenolol in either the apical (open circle) or basal (closed circle) chamber (A and B). An aliquot of buffer was taken periodically from the receiving chamber (100 μl from the basal chamber and 50 μl from the apical chamber), and radioactivity was subsequently measured. The pH of the apical and basal chambers was 6.0 and 7.4, respectively. Permeability of atenolol was calculated using the equation described in the *Materials and Methods* section (C). Intracellular accumulation of atenolol was measured at the end of the 120-minute incubation (D). Data were fitted with linear regression. Transport, permeability, and accumulation in the basal-to-apical direction were compared with that in the apical-to-basal direction ($^{*}P < 0.05$; $^{**}P < 0.01$; $^{***}P < 0.001$). Permeability and accumulation in hOCT2/hMATE1 MDCK cells were compared with that in control cells ($^{\#}P < 0.05$; $^{\#\#}P < 0.01$). Each data point represents the mean ± S.D. A to B, apical to basal; B to A, basal to apical.

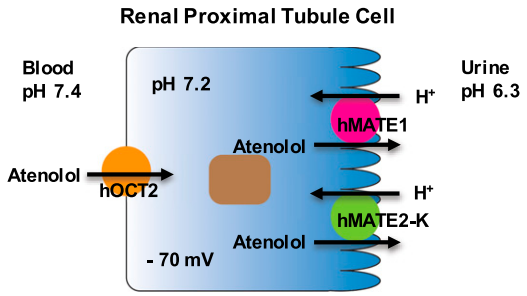

Fig. 8. Proposed scheme of atenolol transport in human renal proximal tubule cells.

carrying a positive charge at the physiologic pH. Detailed kinetic analysis coupled with absolute quantification of transporter protein levels provided further insights into transport efficiencies for individual transporters toward atenolol. While atenolol is an excellent substrate for hOCT1, hOCT2, hMATE1, and hMATE2-K (Figs. 2–4; Tables 1 and 2), hMATE1 appears to transport atenolol with a high affinity but low capacity. In contrast, hOCT2 appeared to be a high capacity and low affinity transporter for atenolol (Tables 1). However, the calculated single transporter transport efficiency (k_{cat}/K_m) was similar for hOCT2 and hMATE1 (Table 2), whereas hOCT1 and hMATE2-K appeared to be 2- to 3-fold more effective. In the human kidney, tubular secretion of the organic cation is mediated by the sequential action of the basolateral hOCT2 and the apical hMATE1 and hMATE2-K. Under nonsaturable conditions, such as those commonly seen in clinical settings, the total transporter-mediated clearance at each membrane domain will be determined by the product of transport efficiency and transporter protein level (i.e., $k_{cat}/K_m \times E_{total}$). The step with lower transport clearance will be rate limiting and will determine if there is intracellular accumulation of the substrate. Indeed, in our hOCT2/hMAT1 double-transfected MDCK cell model, the hOCT2 and hMATE1 protein levels that were determined by LS-MS/MS were 28.6 and 6.9 fmol/μg membrane protein, respectively. The predicted hOCT2-mediated basolateral and hMATE1-mediated apical clearance is 17.0 and 5.3 μl/min per μg membrane protein, respectively, suggesting that hMATE1-mediated apical efflux is the rate-limiting step in atenolol secretion in our in vitro model. Indeed, the much higher intracellular accumulation of atenolol in hOCT2/hMATE1 cells (Fig. 7D) is consistent with our prediction. Currently, the protein expression levels for hOCT2, hMATE1, and hMATE2-K in the human kidney proximal tubule are unknown. If these data become available, it might be possible to predict transporter clearance and the rate-limiting step in atenolol renal secretion in vivo based on individual transporter expression levels and single transporter kinetics of atenolol determined in our study (Table 2). In addition, given the structural similarity of atenolol to other β-blockers, it is reasonable to suspect that the hOCT2/hMATEs secretion pathway may also be involved in renal handling of other hydrophilic β-blockers.

hOCT2 is one of the seven drug transporters currently recommended by the U.S. Food and Drug Administration and the International Transporter Consortium for the evaluation of potential drug interaction risk during drug development (http://www.fda.gov/downloads/Drugs/GuidanceComplianceRegulatoryInformation/Guidances/ucm292362.pdf). hMATE1 and hMATE2-K were recently identified by the International Transporter Consortium as emerging transporters of clinical importance in pharmacokinetics and drug-drug interactions in humans (Hillgren et al., 2013). Metformin, a well established substrate for hOCTs and hMATES, is currently recommended by the U.S. Food and Drug Administration as the probe substrate for in vivo renal DDI studies for hOCT2 (U.S. Food and Drug Administration, 2012). Interestingly, metformin and atenonol share a number of similarities in their physiochemical and pharmacokinetic characteristics (Table 4). Both atenolol and metformin are small hydrophilic cations at the physiologic pH. Atenolol and metformin have similar bioavailabilities (40–60%) and large distributional volumes (Kirch and Gorg, 1982; Scheen, 1996). Both drugs are not protein bound and are exclusively eliminated by the kidney unchanged. Our data demonstrated that similar to metformin, atenolol is actively secreted by the hOCT2/hMATEs pathway (Figs. 6 and 7). Our data revealed that atenolol is an excellent substrate for hOCT2 and hMATE1/hMATE2-K (Figs. 3 and 4) and achieved a B-to-A/A-to-B ratio comparable to metformin in our hOCT2/hMATE1-transfected MDCK cells (Figs. 6 and 7). However, the renal clearance of atenolol (~168 ml/min) is only 1.4-fold of the glomerular filtration clearance (120 ml/min), which is about 3-fold lower than the renal clearance of metformin (Mason et al., 1979; Pentikainen et al., 1979). It is possible that atenolol is efficiently secreted by hOCT2/hMATEs but undergoes substantial reabsorption in the nephron tubules. Metformin, on the other hand, is much less reabsorbed in the nephron. Indeed, atenolol is less hydrophilic than metformin (log $D_{7.4}$: -2.0 versus -5.5) and has a smaller faction of protonization (pKa is 9.6 for atenolol and 12.4 for metformin). Thus, atenolol may undergo passive back diffusion (reabsorption) to a larger extent than metformin in the nephrons. Compared with metformin, few studies reported positive atenolol interactions with prototype renal organic cation transport inhibitors (e.g., cimetidine). This is also likely due to a smaller contribution of secretion clearance to the total renal clearance of the drug. Nevertheless, the efficient transport of atenolol by hOCT2 and hMATEs in vitro and its lower in vivo DDI risk suggest that atenolol may be a useful and clinically relevant substrate for the hOCT2 and hMATE1/hMATE2-K substrate.

Like many β-blockers, atenolol has two enantiomers. Because radiolabeled *R*- or *S*-isomers are not available, we performed inhibition studies with each stereoisomer. Our data suggest that hOCT1, hOCT2, hMATE1, and hMATE2-K do not exhibit pronounced stereoselectivity toward atenolol enantiomers (Fig. 5; Table 3). Our in vitro data are in agreement with clinical observations showing little to a very small difference in the renal clearance of *R*- and *S*-atenolol (Boyd et al., 1989; Mehvar et al., 1990). To date, very few studies reported a stereoselective interaction of organic cations with hOCTs or hMATEs (Zhou et al., 2014). Gross and Somogyi previously evaluated the interaction of the stereoisomers of chiral basic drugs with the uptake of [^{14}C] tetraethylammonium in rat renal membrane vesicles. No differences

TABLE 4

Comparison of the physiochemical properties and human pharmacokinetic parameters for atenolol and metformin

Parameters	Atenolol[a]	Metformin[a]
MW	266	129
Log $D_{7.4}$	−2.0	−5.5
pKa	9.6	12.4
F (%)	52–63	40–60
f_u (%)	> 95	100
V_d (l)	95	63–276
CL (ml/min)	178	459
CL_R (ml/min)	168	454
f_e (%)	> 95	99.9
$t_{1/2}$ (hours)	6	8–20

CL, total plasma clearance; CL_R, renal clearance; *F*, oral bioavailability; f_e, fraction excreted unchanged in urine after i.v. dosing; f_u, plasma unbound fraction; Log $D_{7.4}$, distribution coefficient at pH 7.4; MW, molecular weight; V_d, volume of distribution; $t_{1/2}$, terminal elimination half-life.

[a]The human pharmacokinetic parameters were compiled from Mason et al. (1979), Goodman et al. (2011), Brown et al. (1976), Wadworth et al. (1991), Pentikäinen et al. (1979), and Scheen (1996).

were observed for many enantiomers (Gross and Somogyi, 1994). A small difference was observed only when the center of chirality is adjacent to the basic functional group (Gross and Somogyi, 1994). This is not the case for atenolol as its chiral center is separated from the amine group by one carbon length.

In contrast to a previous study that indicated no transport of atenolol by hOCT1 (Ciarimboli et al., 2013), our data clearly demonstrated that atenolol is an excellent substrate of hOCT1 (Figs. 2 and 3; Tables 1 and 2). The role of hOCT1 in atenolol disposition is currently unclear. hOCT1 is mainly expressed in the sinusoidal membrane of hepatocytes (Giacomini et al., 2010) and is also found in the small intestine (Koepsell et al., 2007). Therefore, this transporter may play a role in the oral absorption and tissue distribution of atenolol. Interestingly, several case reports have described liver injury associated with atenolol use (Schwartz et al., 1989; Yusuf and Mishra, 1995; Dumortier et al., 2009). It would be reasonable to suspect an involvement of hepatic organic cation transporters (e.g., hOCT1 and hMATE1) in atenolol disposition and toxicity in the liver. In addition, atenolol has been reported to be a substrate of OATP1A2 and P-gp (Augustijns and Mols, 2004; Wang et al., 2005; Kato et al., 2009). Therefore, these transporters could also influence atenolol disposition and pharmacokinetics in vivo.

In summary, we showed that atenolol is an excellent substrate for the renal organic cation transporters hOCT2, hMATE1, and hMATE2-K and that atenolol tubular secretion is mediated by the hOCT2/hMATEs secretion pathway. Our studies elucidated the molecular mechanisms involved in the renal handling of atenolol and established the importance of organic cation transporters in the transport and disposition of an important antihypertensive drug. Finally, our data suggest that atenolol could be used as a clinically relevant probe substrate for assessing hOCT1/2 and hMATE1/hMATE2-K function in vitro and in vivo.

Acknowledgments

The authors thank Professor Kazuo Matsubara at the Department of Clinical Pharmacology and Therapeutics, Kyoto University Hospital, for providing the hMATE2-K cDNA plasmid to this study.

Authorship Contributions

Participated in research design: Yin, Wang

Conducted experiments: Yin, Duan, Shirasaka, Prasad

Performed data analysis: Yin, Wang

Wrote or contributed to the writing of the manuscript: Yin, Duan, Prasad, Wang.

References

Agon P, Goethals P, Van Haver D, and Kaufman JM (1991) Permeability of the blood-brain barrier for atenolol studied by positron emission tomography. *J Pharm Pharmacol* **43**:597–600.

Agrawal H, Aggarwal K, Littrell R, Velagapudi P, Turagam MK, Mittal M, and Alpert MA (2015) Pharmacological and non pharmacological strategies in the management of coronary artery disease and chronic kidney disease. *Curr Cardiol Rev* **11**:261–269.

Ahlin G, Hilgendorf C, Karlsson J, Szigyarto CA, Uhlén M, and Artursson P (2009) Endogenous gene and protein expression of drug-transporting proteins in cell lines routinely used in drug discovery programs. *Drug Metab Dispos* **37**:2275–2283.

Ahlin G, Karlsson J, Pedersen JM, Gustavsson L, Larsson R, Matsson P, Norinder U, Bergström CA, and Artursson P (2008) Structural requirements for drug inhibition of the liver specific human organic cation transport protein 1. *J Med Chem* **51**:5932–5942.

Augustijns P and Mols R (2004) HPLC with programmed wavelength fluorescence detection for the simultaneous determination of marker compounds of integrity and P-gp functionality in the Caco-2 intestinal absorption model. *J Pharm Biomed Anal* **34**:971–978.

Avdeef A (2010) Leakiness and size exclusion of paracellular channels in cultured epithelial cell monolayers-interlaboratory comparison. *Pharm Res* **27**:480–489.

Boyd RA, Chin SK, Don-Pedro O, Williams RL, and Giacomini KM (1989) The pharmacokinetics of the enantiomers of atenolol. *Clin Pharmacol Ther* **45**:403–410.

Brown HC, Carruthers SG, Johnston GD, Kelly JG, McAinsh J, McDevitt DG, and Shanks RG (1976) Clinical pharmacologic observations on atenolol, a beta-adrenoceptor blocker. *Clin Pharmacol Ther* **20**:524–534.

Burckhardt G (2012) Drug transport by organic anion transporters (OATs). *Pharmacol Ther* **136**: 106–130.

Ciarimboli G, Schröter R, Neugebauer U, Vollenbröker B, Gabriëls G, Brzica H, Sabolić I, Pietig G, Pavenstädt H, and Schlatter E, et al. (2013) Kidney transplantation down-regulates expression of organic cation transporters, which translocate β-blockers and fluoroquinolones. *Mol Pharm* **10**:2370–2380.

Duan H, Hu T, Foti R, Pan Y, Swaan P, and Wang J (2015) Potent and selective inhibition of plasma membrane monoamine transporter (PMAT) by HIV protease inhibitors. *Drug Metab Dispos* DOI: 10.1124/dmd.115.064824 [published ahead of print].

Duan H and Wang J (2010) Selective transport of monoamine neurotransmitters by human plasma membrane monoamine transporter and organic cation transporter 3. *J Pharmacol Exp Ther* **335**: 743–753.

Dukes JD, Whitley P, and Chalmers AD (2011) The MDCK variety pack: choosing the right strain. *BMC Cell Biol* **12**:43.

Dumortier J, Guillaud O, Gouraud A, Pittau G, Vial T, Boillot O, and Scoazec JY (2009) Atenolol hepatotoxicity: report of a complicated case. *Ann Pharmacother* **43**:1719–1723.

Giacomini KM, Huang SM, Tweedie DJ, Benet LZ, Brouwer KL, Chu X, Dahlin A, Evers R, Fischer V, and Hillgren KM, et al.; International Transporter Consortium (2010) Membrane transporters in drug development. *Nat Rev Drug Discov* **9**:215–236.

Goodman LS, Brunton LL, Blumenthal DK, Murri N, and Hilal-Dandan R (2011) *Goodman & Gilman's The Pharmacological Basis of Therapeutics*, McGraw-Hill Medical, New York.

Gross AS and Somogyi AA (1994) Interaction of the stereoisomers of basic drugs with the uptake of tetraethylammonium by rat renal brush-border membrane vesicles. *J Pharmacol Exp Ther* **268**:1073–1080.

Hernández-Cañero A, González A, Cardonne A, Pérez-Medina T, and Garcia-Barreto D (1972) Effect of atenolol in angina pectoris of effort. *Cor Vasa* **20**:99–103.

Hillgren KM, Keppler D, Zur AA, Giacomini KM, Stieger B, Cass CE, and Zhang L; International Transporter Consortium (2013) Emerging transporters of clinical importance: an update from the International Transporter Consortium. *Clin Pharmacol Ther* **94**:52–63.

Jeon H, Jang IJ, Lee S, Ohashi K, Kotegawa T, Ieiri I, Cho JY, Yoon SH, Shin SG, and Yu KS, et al. (2013) Apple juice greatly reduces systemic exposure to atenolol. *Br J Clin Pharmacol* **75**:172–179.

Kato Y, Miyazaki T, Kano T, Sugiura T, Kubo Y, and Tsuji A (2009) Involvement of influx and efflux transport systems in gastrointestinal absorption of celiprolol. *J Pharm Sci* **98**:2529–2539.

Kirch W and Görg KG (1982) Clinical pharmacokinetics of atenolol–a review. *Eur J Drug Metab Pharmacokinet* **7**:81–91.

Koepsell H, Lips K, and Volk C (2007) Polyspecific organic cation transporters: structure, function, physiological roles, and biopharmaceutical implications. *Pharm Res* **24**: 1227–1251.

König J, Zolk O, Singer K, Hoffmann C, and Fromm MF (2011) Double-transfected MDCK cells expressing human OCT1/MATE1 or OCT2/MATE1: determinants of uptake and transcellular translocation of organic cations. *Br J Pharmacol* **163**:546–555.

Kuteykin-Teplyakov K, Luna-Tortós C, Ambroziak K, and Löscher W (2010) Differences in the expression of endogenous efflux transporters in MDR1-transfected versus wildtype cell lines affect P-glycoprotein mediated drug transport. *Br J Pharmacol* **160**:1453–1463.

Lee N, Hebert MF, Prasad B, Easterling TR, Kelly EJ, Unadkat JD, and Wang J (2013) Effect of gestational age on mRNA and protein expression of polyspecific organic cation transporters during pregnancy. *Drug Metab Dispos* **41**:2225–2232.

Li M, Anderson GD, Phillips BR, Kong W, Shen DD, and Wang J (2006) Interactions of amoxicillin and cefaclor with human renal organic anion and peptide transporters. *Drug Metab Dispos* **34**:547–555.

Lilja JJ, Raaska K, and Neuvonen PJ (2005) Effects of orange juice on the pharmacokinetics of atenolol. *Eur J Clin Pharmacol* **61**:337–340.

Martínez V, Maguregui MI, Jiménez RM, and Alonso RM (2000) Determination of the pKa values of beta-blockers by automated potentiometric titrations. *J Pharm Biomed Anal* **23**: 459–468.

Mason JN, Farmer H, Tomlinson ID, Schwartz JW, Savchenko V, DeFelice LJ, Rosenthal SJ, and Blakely RD (2005) Novel fluorescence-based approaches for the study of biogenic amine transporter localization, activity, and regulation. *J Neurosci Methods* **143**:3–25.

Mason WD, Winer N, Kochak G, Cohen I, and Bell R (1979) Kinetics and absolute bioavailability of atenolol. *Clin Pharmacol Ther* **25**:408–415.

Masuda S, Terada T, Yonezawa A, Tanihara Y, Kishimoto K, Katsura T, Ogawa O, and Inui K (2006) Identification and functional characterization of a new human kidney-specific H +/organic cation antiporter, kidney-specific multidrug and toxin extrusion 2. *J Am Soc Nephrol* **17**:2127–2135.

Mehvar R, Gross ME, and Kreamer RN (1990) Pharmacokinetics of atenolol enantiomers in humans and rats. *J Pharm Sci* **79**:881–885.

Melin K (2014) Antihypertensives, in: *Lippincott Illustrated Reviews: Pharmacology* (Whalen K, Finkel R, and Panavelil T eds), Lippincott Williams & Wilkins, New York.

Morrissey KM, Stocker SL, Wittwer MB, Xu L, and Giacomini KM (2013) Renal transporters in drug development. *Annu Rev Pharmacol Toxicol* **53**:503–529.

Motohashi H and Inui K (2013) Organic cation transporter OCTs (SLC22) and MATEs (SLC47) in the human kidney. *AAPS J* **15**:581–588.

Müller F, König J, Glaeser H, Schmidt I, Zolk O, Fromm MF, and Maas R (2011) Molecular mechanism of renal tubular secretion of the antimalarial drug chloroquine. *Antimicrob Agents Chemother* **55**:3091–3098.

Müller F, König J, Hoier E, Mandery K, and Fromm MF (2013) Role of organic cation transporter OCT2 and multidrug and toxin extrusion proteins MATE1 and MATE2-K for transport and drug interactions of the antiviral lamivudine. *Biochem Pharmacol* **86**:808–815.

Otsuka M, Matsumoto T, Morimoto R, Arioka S, Omote H, and Moriyama Y (2005) A human transporter protein that mediates the final excretion step for toxic organic cations. *Proc Natl Acad Sci USA* **102**:17923–17928.

Pentikäinen PJ, Neuvonen PJ, and Penttilä A (1979) Pharmacokinetics of metformin after intravenous and oral administration to man. *Eur J Clin Pharmacol* **16**:195–202.

Poirier L and Lacourcière Y (2012) The evolving role of β-adrenergic receptor blockers in managing hypertension. *Can J Cardiol* **28**:334–340.

Prasad B and Unadkat JD (2014) Optimized approaches for quantification of drug transporters in tissues and cells by MRM proteomics. *AAPS J* **16**:634–648.

Roland M and Tozer TN (2010) *Clinical Pharmacokinetics and Pharmacodynamics: Concepts and Applications*, LWW, Baltimore.

Sato T, Masuda S, Yonezawa A, Tanihara Y, Katsura T, and Inui K (2008) Transcellular transport of organic cations in double-transfected MDCK cells expressing human organic cation transporters hOCT1/hMATE1 and hOCT2/hMATE1. *Biochem Pharmacol* **76**:894–903.

Scheen AJ (1996) Clinical pharmacokinetics of metformin. *Clin Pharmacokinet* **30**:359–371.

Schwartz MS, Frank MS, Yanoff A, and Morecki R (1989) Atenolol-associated cholestasis. *Am J Gastroenterol* **84**:1084–1086.
Shu Y, Bello CL, Mangravite LM, Feng B, and Giacomini KM (2001) Functional characteristics and steroid hormone-mediated regulation of an organic cation transporter in Madin-Darby canine kidney cells. *J Pharmacol Exp Ther* **299**:392–398.
Tabacova SA and Kimmel CA (2002) Atenolol: pharmacokinetic/dynamic aspects of comparative developmental toxicity. *Reprod Toxicol* **16**:1–7.
Tsuda M, Terada T, Ueba M, Sato T, Masuda S, Katsura T, and Inui K (2009) Involvement of human multidrug and toxin extrusion 1 in the drug interaction between cimetidine and metformin in renal epithelial cells. *J Pharmacol Exp Ther* **329**:185–191.
Wadworth AN, Murdoch D, and Brogden RN (1991) Atenolol. A reappraisal of its pharmacological properties and therapeutic use in cardiovascular disorders. *Drugs* **42**:468–510.
Wang Q, Rager JD, Weinstein K, Kardos PS, Dobson GL, Li J, and Hidalgo IJ (2005) Evaluation of the MDR-MDCK cell line as a permeability screen for the blood-brain barrier. *Int J Pharm* **288**:349–359.
World Health Organization (2011) *Causes of Death 2008*, World Health Organization, Geneva, Switzerland.
You G (2004) The role of organic ion transporters in drug disposition: an update. *Curr Drug Metab* **5**:55–62.
Yusuf SW and Mishra RM (1995) Hepatic dysfunction associated with atenolol. *Lancet* **346**:192.
Zhou Q, Yu LS, and Zeng S (2014) Stereoselectivity of chiral drug transport: a focus on enantiomer-transporter interaction. *Drug Metab Rev* **46**:283–290.

Address correspondence to: Dr. Joanne Wang, University of Washington, Department of Pharmaceutics, H272J Health Sciences Building, Seattle, WA 98195-7610. E-mail: jowang@uw.edu